scientific reports

Check for updates

OPEN

Gallic acid alleviates ferroptosis by negatively regulating APOC3 and improves nerve function deficit caused by traumatic brain injury

Yu Liu[1,3], Xiaojia Fu[1,2,3], Jing Li[1,3], Jianqiang Guo[1,2], Zongren Zhao[1]✉ & Jinyu Zheng[1]✉

Traumatic brain injury (TBI) is more common than ever and is becoming a global public health issue. A variety of secondary brain injuries occur after TBI, including ferroptosis characterized by iron-dependent lipid peroxidation. Gallic acid is a kind of traditional Chinese medicine, which has many biological effects such as anti-inflammatory and antioxidant. We further investigated whether Gallic acid can improve the neurological impairment caused by ferroptosis after TBI by targeting APOC3. Weighted gene coexpression network analyses (WGCNA) and 3 kinds of machine-learning algorithms were used to find the potential biomarkers. Then the HERB database was used to select the Chinese herb that acted on the target gene APOC3. Finally, we selected Gallic acid as a drug targeting APOC3 and verified by Western blotting. The effect of Gallic acid on the improvement of neurological function was studied by Nissl staining and FJB staining. Finally, the effect of Gallic acid on the cognitive ability of TBI mice was explored through behavioral experiments. Gallic acid can inhibit the expression level of APOC3 and thus inhibit the level of ferroptosis after TBI. It can also reduce the degeneration of nerve tissue by inhibiting ferroptosis and improve the neurological function deficit. The behavioral experiment proved that Gallic acid can alleviate the behavioral cognitive impairment caused by TBI. Gallic acid can reduce ferroptosis by inhibiting APOC3, and then alleviate neurological impairment after TBI.

Keywords Gallic acid, APOC3, Traumatic brain injury, Machine-learning algorithm, Ferroptosis

TBI is a major global health problem and a leading cause of death and disability[1]. It occurs as a result of direct impact or impact to the head from factors such as motor vehicles, crush and assault[2]. Even non-fatal injuries can lead to severe lifelong disability, which has significant implications for the injured and their families, as well as for medical costs[3–5]. The damage caused by TBI to brain tissue can be divided into primary damage and secondary damage. There are many forms of secondary brain injury, including brain tissue edema, blood brain barrier (BBB) destruction, reactive oxygen species (ROS) production and inflammation[6–8]. Cell death can be divided into apoptosis, necrosis, autophagy and ferroptosis[9,10]. Active intervention to the secondary injury of TBI can improve the neurological impairment and improve the prognosis of patients[11].

Ferroptosis is a new type of cell death discovered in recent years[12]. It is a kind of oxidative cell death induced by small molecules, which is iron ion dependent[13]. Its occurrence is caused by the imbalance between the generation and degradation of intracellular lipid reactive oxygen species[14]. Ferroptosis inducers directly or indirectly act on glutathione peroxidase (GPXs) through different pathways, leading to the reduction of cellular antioxidant capacity, ROS accumulation, and finally oxidative cell death[15–17]. Ferroptosis is not only related to the occurrence and development of TBI, but the key proteins in the related signaling pathway can also become targets for drug action[18–20].

In this study, we performed gene expression level analysis on the downloaded dataset to obtain differentially expressed genes between TBI patients and normal subjects. Combined the downloaded data with WGCNA and machine-learning algorithm including Support Vector Machines (SVM), least absolute shrinkage and selection operator (LASSO) regression, and Random Forest (RF)[21–23]. Ultimately, we screened out the differentially expressed genes between normal brain tissue and TBI brain tissue for further study. Using the HERB database, a specialized Chinese medicine high-throughput experimental and reference database, the Chinese herb (fruit of

[1]Department of Neurosurgery, The Affiliated Huai'an Hospital of Xuzhou Medical University, Huai'an 223022, China. [2]Xuzhou Medical University, Xuzhou 221000, China. [3]Yu Liu, Xiaojia Fu and Jing Li contributed equally. ✉email: zhaozongrenking@163.com; guanr80@163.com

Axillary choerospondias) that acts on the target gene was selected[24]. Fruit of Axillary choerospondias is the dried and mature fruit of Southern Jujube, a plant in the Urticaceae family[25]. Its main component contains Gallic acid, chemical name is 3, 4, 5-trihydroxybenzoic acid, molecular formula $C_7H_6O_5$, which is a polyphenolic organic compound[26]. Gallic acid has anti-inflammatory, anti-mutation, anti-oxidation, anti-free radical and other biological activities, and these biological activities are closely related to the secondary damage after TBI, which is considered to be the potential mechanism of its treatment of TBI[27]. Previous studies have shown that Gallic acid can improve the neurological deficit after TBI through anti-inflammatory and antioxidant, but whether it can treat TBI by anti-ferroptosis has not been reported[28].

In order to clarify the effect of Gallic acid on ferroptosis in brain tissue caused by TBI, we first explored the effect of Gallic acid on the expression level of key protein of ferroptosis. Then, the characteristic changes of ferroptosis in mitochondria were observed under electron microscope, and iron deposition levels in tissues were detected by Perl's staining to further verify the inhibitory effect of Gallic acid on ferroptosis. Finally, the protective effect of Gallic acid on neural function and behavioral cognition after TBI was confirmed through the neurodegeneration level and animal behavior experiments.

Materials and methods

Data collection and potential drugs screening

The gene expression profile (GSE2871) was obtained from the GEO database (https://www.ncbi.nlm.nih.gov/geo/), which was sequenced using the GPL85 platform. At early post-injury timepoint, animals will be sacrificed, brain regions (parietal cortex and hippocampus, ipsilateral and contralateral to injury) will be dissected and RNA isolated. RNA will be used to synthesize cRNA probes for microarray hybridization. We identified a number of potential drugs that may act on some of the TBI-associated genes identified in this study in the HERB database (http://herb.ac.cn/) and other public databases (https://drugcentral.org/).

Identiffication of DEGs and GSEA

The "Limma" R package was used to screen differentially expressed genes (DEGs) between TBI and normal samples, and genes with $P < 0.05$ and $|\log2FC| > 1$ were regarded as DEGs. GSEA-4.1.0 was used to input the expression data and phenotypic data, and the five most significantly up-regulated pathways and the most significantly down-regulated pathways were plotted, respectively.

Screening of the critical genes

To find out the core genes that were altered after TBI, the downloaded dataset was used to construct a weighted gene co-expression network using the "WGCNA" R package. Then, we performed a cluster analysis of the samples and calculated the pearson correlation coefficient between each pair of genes to evaluate the expression similarity of genes and acquire a correlation matrix. We further used a soft threshold function to transform the correlation matrix into a weighted neighborhood matrix, and a soft join algorithm was used to select the optimal soft threshold to ensure that gene correlations fit the scale-free distribution to the greatest extent possible. Subsequently, the neighborhood matrix was transformed into a topological overlap matrix. After obtaining the co-expression modules, the key modules were screened out by correlation analysis, and the genes of the key modules were regarded as the key genes. Based on WGCNA screening, DEGs and key genes were intersected to obtain the target genes.

Identification of TBI hub genes based on machine-learning algorithms

Least absolute shrinkage and selection operator (LASSO) is a regression analysis method that performs both gene selection and classification[13]. First, the R package glmnet (Version4.1.2) was used to fit the logistic LASSO regression model. Next, the SVM-RFE algorithm was used to screen potential genes using the "e1071" R package. In addition, the random forest (RF) algorithm was also conducted to screen potential genes using the "randomForest" R package. Finally, the intersection of the genes obtained by LASSO, SVM-RFE and RF machine-learning algorithms was taken by Veen graph as the hub genes of TBI.

Experimental animals and grouping

The male ICR mice (6–8 weeks, 20–30 g) used in this experiment were purchased from Hangzhou Ziyuan Experimental Animal Technology Co., LTD., and fed in the mouse house for 7 days for the experiment. The temperature of the mouse house is controlled at 22 ~ 25°C, the humidity is 70% ~ 75%, and the water and food are adequately supplied. All animal experiments were conducted in accordance with the animal welfare policy of The Affiliated Huai'an Hospital of Xuzhou Medical University and were approved by The Affiliated Huai'an Hospital of Xuzhou Medical University. The experimental animals were randomly divided into Sham group, TBI group and TBI + Gal group (Gallic acid, 40 mg/kg, ip). In Sham group, the bone window was opened but not traumatized. The TBI group was traumatized but not treated. Gallic acid (MedChemExpress, USA) is administered once 30 min after TBI and then once daily. The experimental section of this study fully complies with the ARRIVE guidelines.

The construction of TBI model

The Feeney free-fall impact method was used to construct the TBI model[29]. First, the mice were anesthetized with isoflurane by an inhalation anesthesia machine (M5209, Changsha Maiyue Biotechnology Co., Ltd.) and fixed in a stereoscope, then the local hair was removed and disinfected with iodophor. Then the scalp was cut about 1.5 cm along the median line of the mouse skull, exposing the skull and stripping the periosteum. Drilling was then done with a 2 mm diameter cranial rotatory to create a bone window of about 5 mm diameter, exposing the parietal lobe with as little damage to the dura as possible. Parameters for setting up the craniocerebral injury

percussion apparatus are as follows: weight mass 20 g, drop height 15 cm, impact depth 1.5 mm. After the attack, the mice were hemostatic and the scalp was tightly sutured, and then returned to the original cage for feeding. All operations should pay attention to the principle of asepsis, and the instruments should be autoclaved and disinfected in advance during the operation.

Quantitative real-time PCR

Total RNA extraction and cDNA reverse transcription of mouse brain tissue were performed by the Vazyme (Vazyme Biotech, Nanjing, China) kit. Using GAPDH as internal parameter, $2^{-\Delta\Delta Ct}$ method was used to calculate the expression levels. Primer sequences for target genes:

STK39 (Forward)5' - CAAACCCAGGCAAGAACGC – 3' ;
STK39 (Reverse)5' - GCCACAGCTCATCTTTGACCAC – 3' ;
Kcnd3 (Forward)5' - CACCAGTCGCTCCAGCCTTAA – 3' ;
Kcnd3 (Reverse)5' - GACGACATTGCTGGTTATGGAAG – 3' ;
Apoc3 (Forward)5' - GAGTCCGATATAGCTGTGGTGG – 3' ;
Apoc3 (Reverse)5' - GTTGGTTGGTCCTCAGGGTTAG – 3' ;
FOXE3 (Forward)5' - CGACTGTTTCGTCAAGGTGC – 3' ;
FOXE3 (Reverse)5' - CGTTGTCGAACATGTCAGCG – 3' ;
CHRNB1 (Forward)5' - CCGTTATCCTTAGTGTTGTGGTC – 3' ;
CHRNB1 (Reverse)5' - AGTGATGTGGTTCAGGGAGTTG – 3' ;
NPW (Forward)5' - CTGCTAGAGCCTTCGGAGAGAC – 3' ;
NPW (Reverse)5' - ATCGGTTCTTGGGCCTGACA – 3' ;
GAPDH (Forward)5' - CCTCGTCCCGTAGACAAAATG – 3' ;
GAPDH (Reverse)5' - TGAGGTCAATGAAGGGGTCGT – 3' .

Western blotting

The tissue blocks were washed with pre-cooled PBS for 2–3 times to remove the blood stain, cut into small pieces and placed in a homogenizing tube. 2 homogenizing beads of 4 mm were added, and the lysate of 10 times the tissue volume was added (protease inhibitor was added before use), and homogenizing procedure was set for homogenizing. Take out the homogenated tube, place the ice lysate for 30 min, and shake every 5 min to ensure complete tissue cracking; The supernatant was collected by centrifugation at 12,000 rpm at 4℃ for 10 min. Protein concentration was quantified using the protein quantification kit (Servicebio, China). Add a certain amount of loading buffer and boil at 95℃ for 10 min to complete sample preparation. Then the sample is applied and electrophoresis is performed successively until the sample reaches the lower edge of the gel. Then the gel was transferred and closed for 1 ~ 2 h. After closure, the primary antibody was incubated overnight (4℃). The next day, the secondary antibody was washed three times with PBS buffer for 5 min each time, and then added to the incubator and incubated at room temperature for 30 min; And then clean it again with PBS buffer for three times, 10 min each time. Luminescent solution (Servicebio, China) was configured and protein band detection and gray scale analysis were performed by imaging system (CLINX, China). The main reagents include primary antibody TfR1 (1:1000, Proteintech, USA), NOX2 (1:1000, Proteintech, USA) and GPX4 (1:1000, Proteintech, USA), secondary antibody Polyclonal Goat Anti-Mouse IgG labeled by HRP (1:2000, Servicebio, China), HRP labeled goat anti-Rabbit secondary antibody (1:2000, Servicebio, China).

Transmission electron microscopy

2 mm brain tissue around the site of brain injury and normal brain tissue at the same site were cut into $1mm^3$ and immersed in electron microscope fixative (G1102-100ML, Servicebio, China). The tissue blocks were fixed at room temperature for 2 h away from light, and then stored in a refrigerator at 4℃. After the tissue blocks were removed, the surface fixing solution was washed with PBS (PH = 7.4) for 3 times, and the washing time was 15 min each time. The rinsed tissue blocks were fixed with 0.1 mol/L PBS (PH = 7.4) prepared with 1% osmic acid and then placed in a dark room at room temperature for 2 h. After that, the tissue blocks were rinsed with PBS (PH = 7.4) for 3 times, and each rinsing time was 15 min. Finally, different concentrations of ethanol and 100% acetone were dehydrated. After completing the above operations, the tissue was sliced with a thickness of 60–80 nm. The tissue sections were double-stained with uranium lead and then left to dry overnight at room temperature. Finally, the sections were analyzed under transmission electron microscopy.

Immunohistochemistry

We first dewaxed the tissue sections according to the previous experimental procedures[30]. After rinsing with PBS for three times, it was incubated in hydrogen peroxide solution in the dark, and then rinsed with PBS solution for three times. The tissue was uniformly covered with 3% BSA in the tissue chemical circle and closed at room temperature for 30 min. The main reagents include primary antibody TfR1 (1:1000, Proteintech, USA), NOX2 (1:1000, Proteintech, USA) and GPX4 (1:1000, Proteintech, USA). After adding the primary antibody, place it in a refrigerator at 4 °C overnight and rinse it the next day. After rinsing the primary antibody and adding the second antibody, incubate in room temperature for 50 min. Secondary antibody Polyclonal Goat Anti-Mouse IgG labeled by HRP (1:2000, Servicebio, China), HRP labeled goat anti-Rabbit secondary antibody (1:2000, Servicebio, China). After completing the above steps, retain the core by DAB color development method for 3 min and then rinse. Then wash with hematoxylin differentiation solution and then rinse with water, and finally, hematoxylin is rinsed after returning to blue. In the last step, the sections were dehydrated in anhydrous ethanol and closed under a microscope.

Perl's staining
First, the paraffin sections of the brain tissue were dewaxed to water. Prepare the Prussian blue dye, add it to the section and dye for 1 h. Then use distilled water to wash the excess dye on the surface of the section. The sections were stained with nuclear fast red staining solution for 3 min and then the excess dye solution was rinsed. Finally, the slices are dehydrated and sealed with neutral gum. Image J 1.53 software was used for image processing.

Nissl staining
The paraffin sections were dewaxed to water and then washed 3 times with PBS. The slices were then incubated by Nissl staining solution (Beyotime Biotechnology, China) for 10 min. The analysis results were photographed with an optical microscope (Nikon 80 i, Japan).

Fluoro-Jade B staining
First, the paraffin sections are dewaxed to water, and then the FJB working liquid is added. The specific process was as follows: the pen circle was organized, 50% ice acetic acid was used as solvent, FJB working liquid (Merck, Germany) was configured at 1: 400, the diluted FJB green fluorescent probe was added, and the nucleus was re-dyed with DAPI after 4°C overnight. Images were collected after sealing.

Lesion degree assessment
We first stained the tissue with HE. The simple process is as follows: (1) Dewaxing paraffin sections to water; (2) Hematoxylin staining; (3) eosin staining; (4) dehydration seal. We started the section from the defect edge to the normal tissue edge with a thickness of 30 μm. Then the brain tissue defect volume was calculated using NIH Image J software (Bethesda, MD, USA).

Evans blue extravasation assay
We measured the amount of EB dye in mouse brain tissue 3 days after TBI to assess the extent of BBB destruction. In simple terms, after injecting EB dye (2%, 2 μL/g) through the tail vein, the mice were anesthetized and then injected with PBS through the left ventricle of the heart to eliminate the localized dye from the sinus bleeding. The brain tissue was then weighed, then the sample was soaked in formamide solution and homogenized at a concentration of 200 mg of tissue per milliliter. 37°C warm bath for 48 h, centrifuge at 6000 rpm for 20 min and remove the supernatant. The absorbance of the mixture at 632 nm was measured using a spectrophotometer (BioTek, Winooski, VT, USA).

Behavioral experiments
The perception and memory abilities of mice were investigated using the Novel Object Recognition (NOR) experiment[31]. Within 3 days of the training stage, an identical object (yellow cube) was placed in a box (100 cm in diameter and 50 cm in height) at a position 20 cm away from the wall, and then the mouse was placed in the middle of the two objects for it to explore by itself. In the experiment phase, a familiar object (yellow cube) was replaced with a new object (white cylinder), and then the mouse was placed in the middle of the two objects and allowed to explore freely for 5 min. New object recognition rate (NORI): the proportion of old object recognition time to all object recognition time.

The Morris water maze experiment is divided into training and experimental stages[30]. The whole process was recorded and evaluated using a video tracking system (Anhui Zhenghua Biological Instrument Equipment Co., LTD. : Huaibei, China). Specific experiments are as follows: During the training phase (the first 7 days), 4 training sessions are performed daily. The mice were randomly placed into the water from a quadrant facing the wall of the pool. If the mouse successfully found the platform within 90 s, it was allowed to stay on the platform for 10 s, and if the mouse failed to find the platform within the specified time, it was guided to the platform for 10 s with a guide stick. The water temperature was kept at 24°C during the experiment. In the experimental stage (day 8 of the water maze test), the platform was removed from the water, and the mice were put into the pool from the opposite quadrant of the platform for a single test. Each mouse swam for 90 s. The movement track of the mice, the number of times they crossed the platform and the time they stayed in the quadrant where the platform was located were recorded.

Statistic analysis
Statistical analyses were performed and plotted using GraphPad Prism 8.4.2 software (San Diego, CA, USA) and SPSS 20.0. Data were presented as means ± SD. (*$P<0.05$, **$P<0.01$, ***$P<0.001$).

Results
Screening of key modules and genes based on WGCNA and machine-learning algorithms
To explore biomarkers that are altered after TBI, this study retrospectively analyzed data on gene expression from TBI and normal samples in GSE2871 by setting the cut-off value as $P<0.05$ and $|\log2FC|>1$. 107 DEGs were identified, including 47 up regulated genes and 60 down regulated genes (Fig. 1A, B). Analysis was performed to identify differentially expressed genes between TBI patients and normal controls. First of all, the soft threshold was selected for subsequent co-expression network construction (Fig. 1C, D). The essence was to make the constructed network more consistent with the characteristics of scale-free networks. WGCNA was used to construct a co-expression network module and visually display the gene correlation of the modules. Co-expression modules were shown in a hierarchical cluster plot (Fig. 1E). Multiple modules were shown to be associated with TBI through the moduletrait correlation studies. Each cell contains the corresponding correlation and *P*-value (Fig. 1F). We show the association between module membership and gene importance using scatter plots (Fig. 1G). The module "MEturquoise" had high association with TBI and was selected as TBI

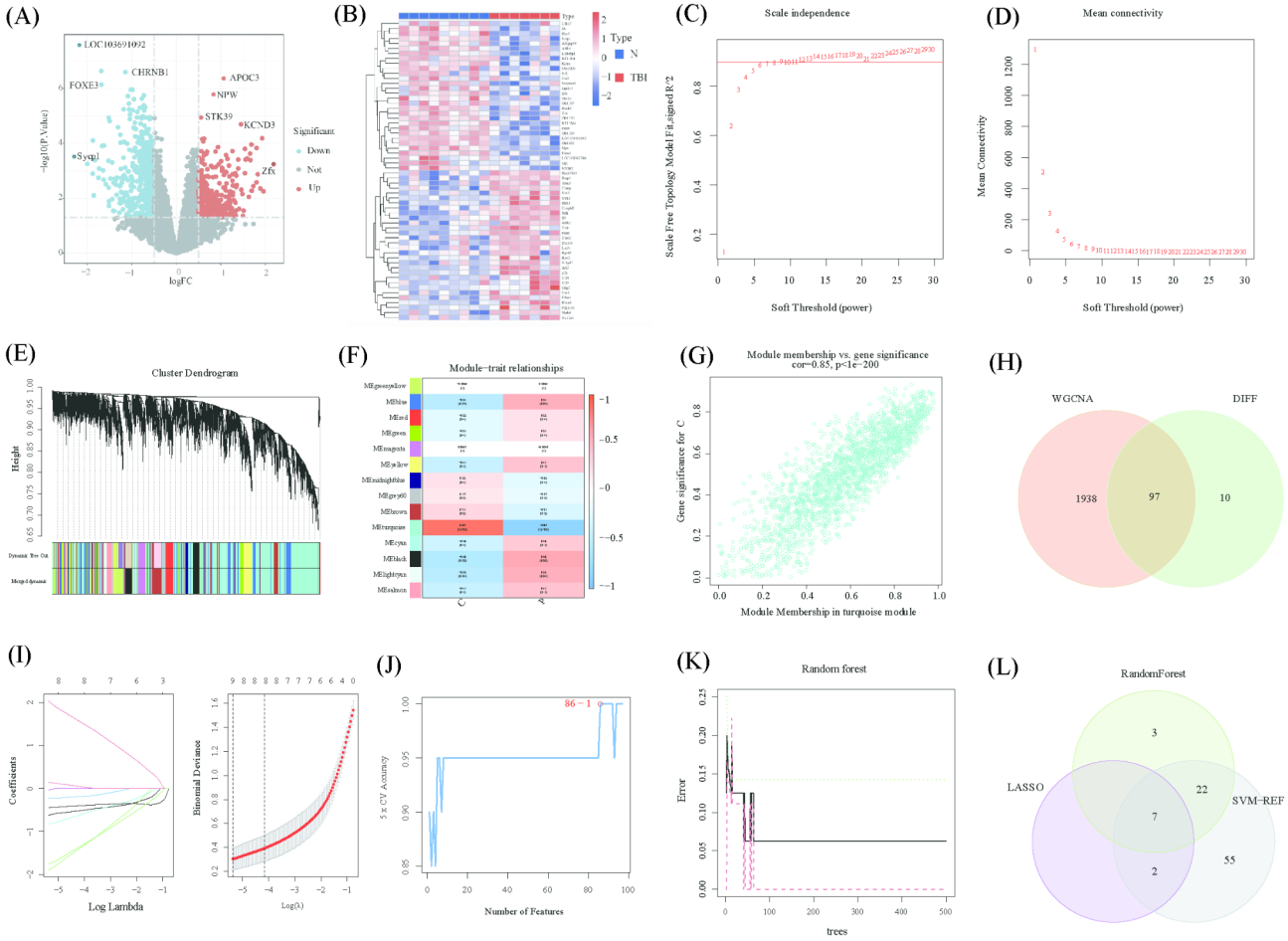

Fig. 1. Screening of key modules and genes based on WGCNA and machine-learning algorithms. (**A**) Volcano plot of DEGs. (**B**) Heat map of DEGs. (**C**, **D**) The soft threshold was selected for subsequent co-expression network construction. (**E**) The cluster dendrogram of co-expression genes in TBI. (**F**) The module-trait relationship heat map. (**G**) Associations between module membership and gene importance is depicted in a scatter plot. (**H**) A Venn diagram was made to obtain the intersection of the target genes screened by the two methods. (**I**) The Log (Lambda) value of the genes in the LASSO model and the most proper log (Lambda) value in the LASSO model. (**J**) The optimum accuracy rate of the SVM model based on the characteristic genes. (**K**) The RF module based on the characteristic genes. (**L**) The Venn diagram showing the overlapping genes in LASSO, SVM, and RF modules.

related module. By WGCNA screening, DEGs were crossed with key genes to obtain target genes (Fig. 1H). To further identify the hub genes of TBI, we selected three machine-learning algorithms to screen the target genes. The LASSO regression approach was used to narrow down the nine overlapping features, and nine variables were were further used in subsequent analyses (Fig. 1I). The SVM-RFE analysis showed that a total of 86 potential genes were identified when the accuracy of SVM model was the best (Fig. 1J). Meanwhile, the RF algorithm identified 32 genes at the lowest error rate (Fig. 1K). Finally, seven hub genes changed after TBI were obtained according to the above three machine-learning algorithms, which were STK39, KCND3, APOC3, FOXE3, CHRNB1, LOC103691092 and NPW (Fig. 1L).

Analysis of core genes and screening of potential drugs

In view of the relatively small sample size and low confidence of the screened gene set, we further verified the meaningful genes by conducting q-PCR analysis on TBI mice. The results showed that only APOC3 and KCND3 had significant differences as well as the screened gFig. (Fig. 2A). The pathophysiological changes after TBI included ROS production, edema, inflammation, angiogenesis and metabolic related changes. We performed ssGSEA on the seven genes, and the results showed that these genes were closely related to these pathophysiology ofFig. (Fig. 2B). We looked at the previous literature and found, the formation of ROS is closely related to FOXE3, CHENB1 and APOC3. Otherwise, APOC3 is closely related to inflammation caused by TBI. We identified a number of potential drugs that may act on some of the TBI-associated genes identified in this study in HERB database and the other public dataFig. (Fig. 2C). In view of the consistency of the results of the previous bioinformatics analysis and q-PCR experiment, as well as its rich role in various pathological processes,

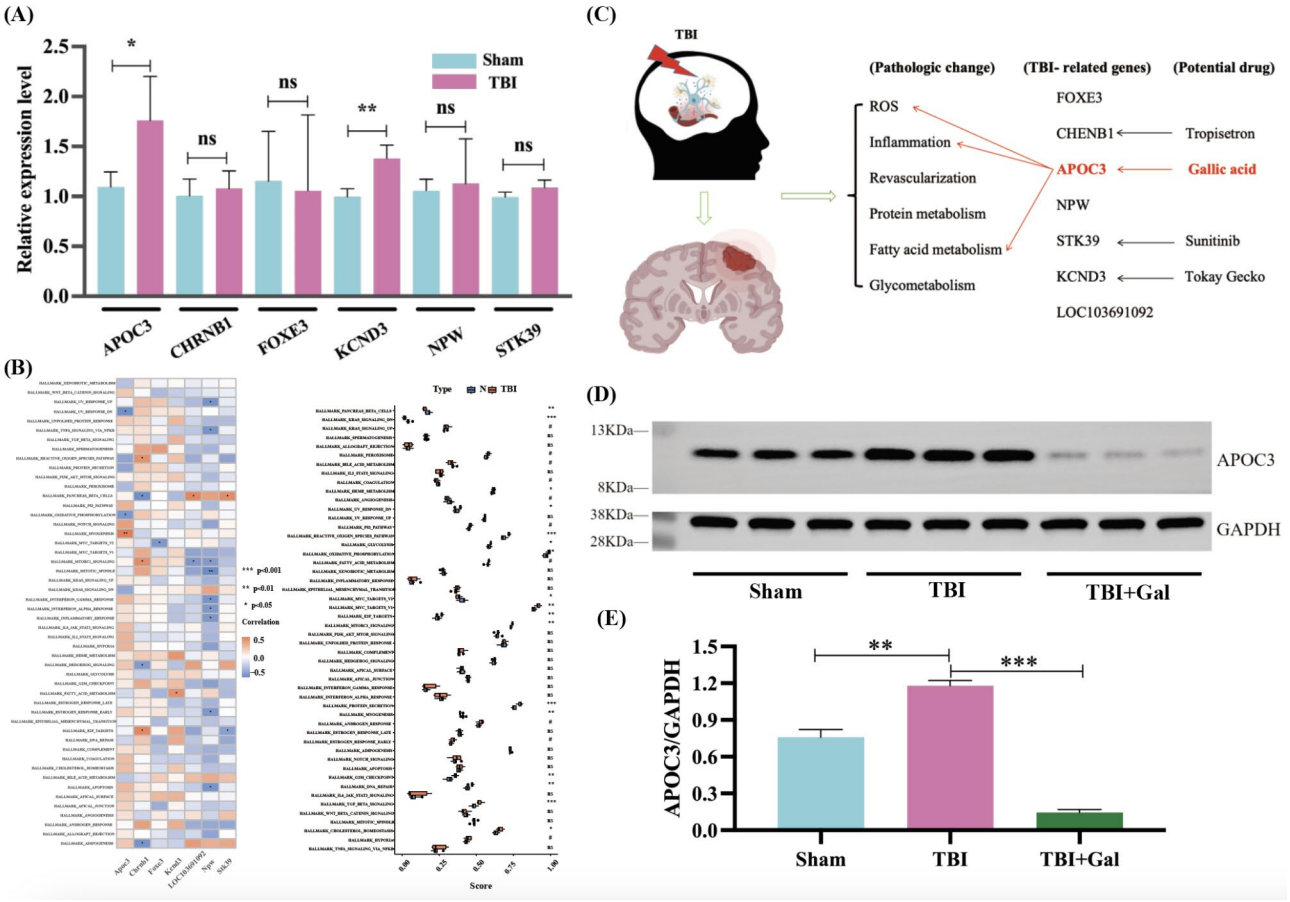

Fig. 2. Screening of core genes and potential drugs. (**A**) q-PCR results of core genes. (**B**) Differential expression of core gene-enriched pathways. (**C**) Potential drugs and regulated pathological processes. (**D**) The expression levels of APOC3 in different groups. (*$P<0.05$, **$P<0.01$, and ***$P<0.001$).

APOC3 was selected for subsequent research.We found Gallic acid acting on APOC3 in the HERB database. Western blotting results showed that Gallic acid could inhibit the increase of APOC3 afterFig. (Fig. 2D, E).

Gallic acid alleviates ferroptosis in brain tissue of TBI mice by inhibiting APOC3

Analysis of the correlation between APOC3 and key protein of iron death from STRING (https://cn.string-db.org) : Protein-Protein Interaction (PPI network) database found that it was closely related to GPX4, NOX2 and Fig. (Fig. 3A). The characteristic changes of mitochondrial ferroptosis were observed under electron microscopy, and it was found that the mitochondrial membrane shrank and mitochondrial ridge disappeared after TBI, and the number of mitochondria with characteristic damage of ferroptosis in the brain tissue of TBI mice after Gallic acid treatment was improved compared with that in the TBI gFig. (Fig. 3B). Further Western blotting results showed that the expression level of GPX4 in brain tissue after TBI was decreased, and the expression level of GPX4 in brain tissue after Gallic acid treatment was significantly increased. The expression levels of NOX2 and TfR1 in the TBI group were higher than those in the normal brain tissue, and the expression levels of NOX2 and TfR1 in the Gallic acid treatment group were significantly lower than those in the TBI gFig. (Fig. 3C-F). The immunohistochemical results were consistent with those of Western blotting, confirming that Gallic acid could inhibit the level of iron death afterFig. (Fig. 3G-J). Perl's staining showed increased iron deposits in TBI tissues and decreased iron deposits in the brain tissues of mice treated with Gallic Fig. (Fig. 3K, L).

Gallic acid alleviates the neurodegeneration caused by TBI

To determine the degree of neuronal necrosis and degenerative changes after TBI, we analyzed the level of neuronal necrosis in brain tissues through Nissl staining. Results showed that the number of normal neurons decreased after TBI, and the degree of neuronal necrosis in the Gallic acid treatment group was lower than that in the TBI gFig. (Fig. 4A, C). The deformed neurons were labeled by FJB staining, and the number of denatured neurons increased after TBI, while the number of denatured neurons decreased after Gallic acid treatFig. (Fig. 4B, D). Then the degree of tissue defect was analyzed by HE staining, and the results showed that the degree of brain tissue defect in the Gallic acid treatment group was lighter than that in the TBI gFig. (Fig. 4E, G). We further studied the effect of Gallic acid on BBB after TBI. Evans blue extravasation assay showed that Gallic acid could improve BBB damage caused by TBI. Reduced Evans blue exudation in brain tiFig. (Fig. 4F, H).

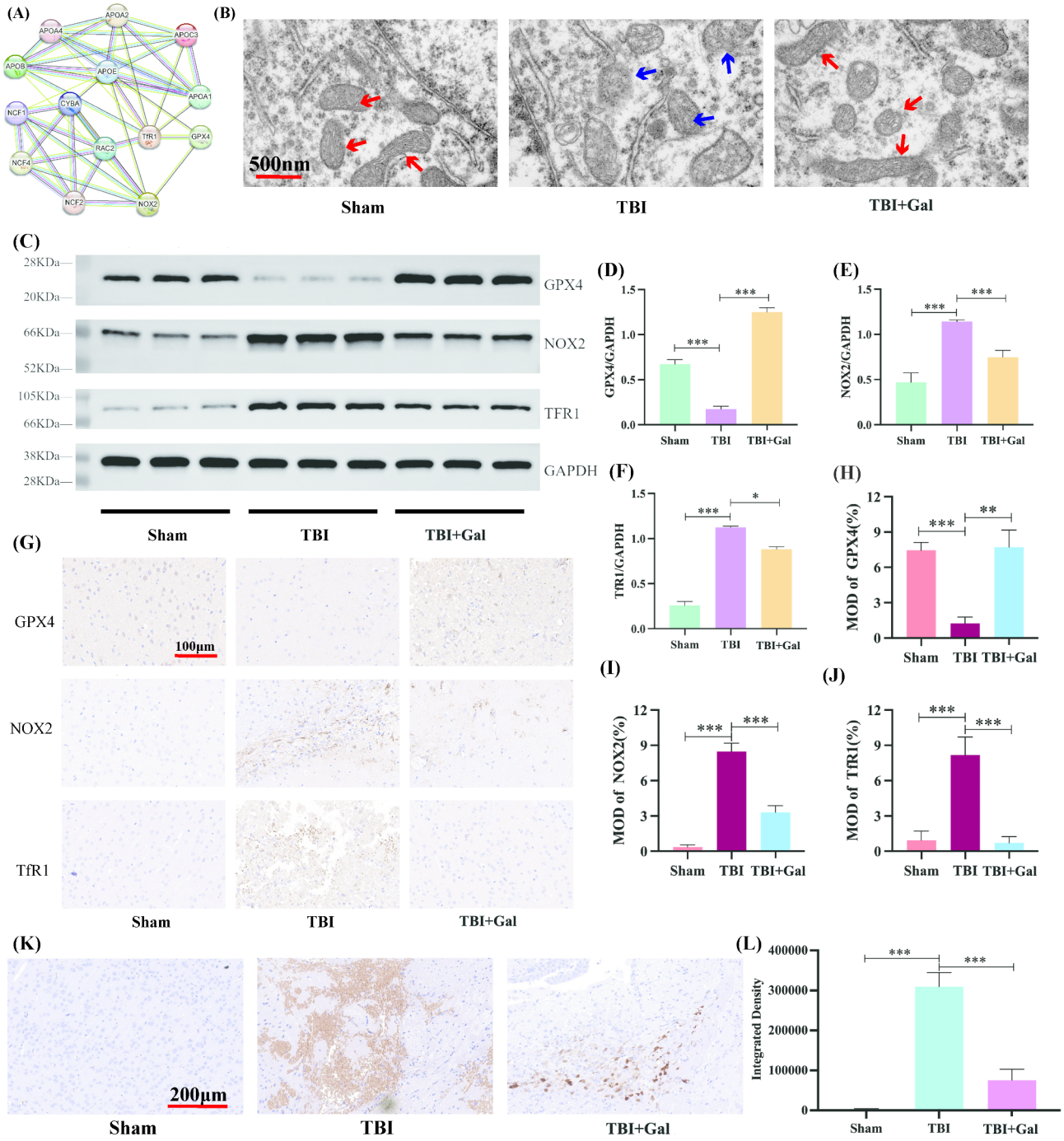

Fig. 3. Gallic acid alleviates ferroptosis caused by TBI. (**A**) PPI analysis of APOC3 and key protein of ferroptosis. (**B**) Changes of mitochondria under electron microscope. (**C**) The expression levels of GPX4, NOX2 and TfR1 were detected by Western blotting. (**D**-**F**) Quantitative analysis of Western blotting results of GPX4, NOX2 and TfR1. (**G**) Representative images of immunohistochemical staining of GPX4, NOX2 and TfR1 in the injured cortex. (**H**-**J**) Quantitative analysis of immunohistochemical staining. (**K**) Representative images of Perl's staining in each group. (**L**) Quantitative analysis of iron deposition level in tissues. (*$P<0.05$, **$P<0.01$, and ***$P<0.001$).

Gallic acid alleviates neurologic deficits and behavioral cognitive impairment caused by TBI

The effect of Gallic acid on the neurological impairment and behavioral cognitive impairment caused by TBI was investigated through behavioral experiments. mNSS scores were performed on day 1, day 3, day 7 and day 14 after TBI, and the differences among all groups were compared on day 14. The Morris water maze experiment was carried out on mice at days 14–21. NOR experiment was performed on the 28th day after TBI. The timeline and schematic of behavioral experiments are shown bFig. (Fig. 5A). The mNSS score results showed that the

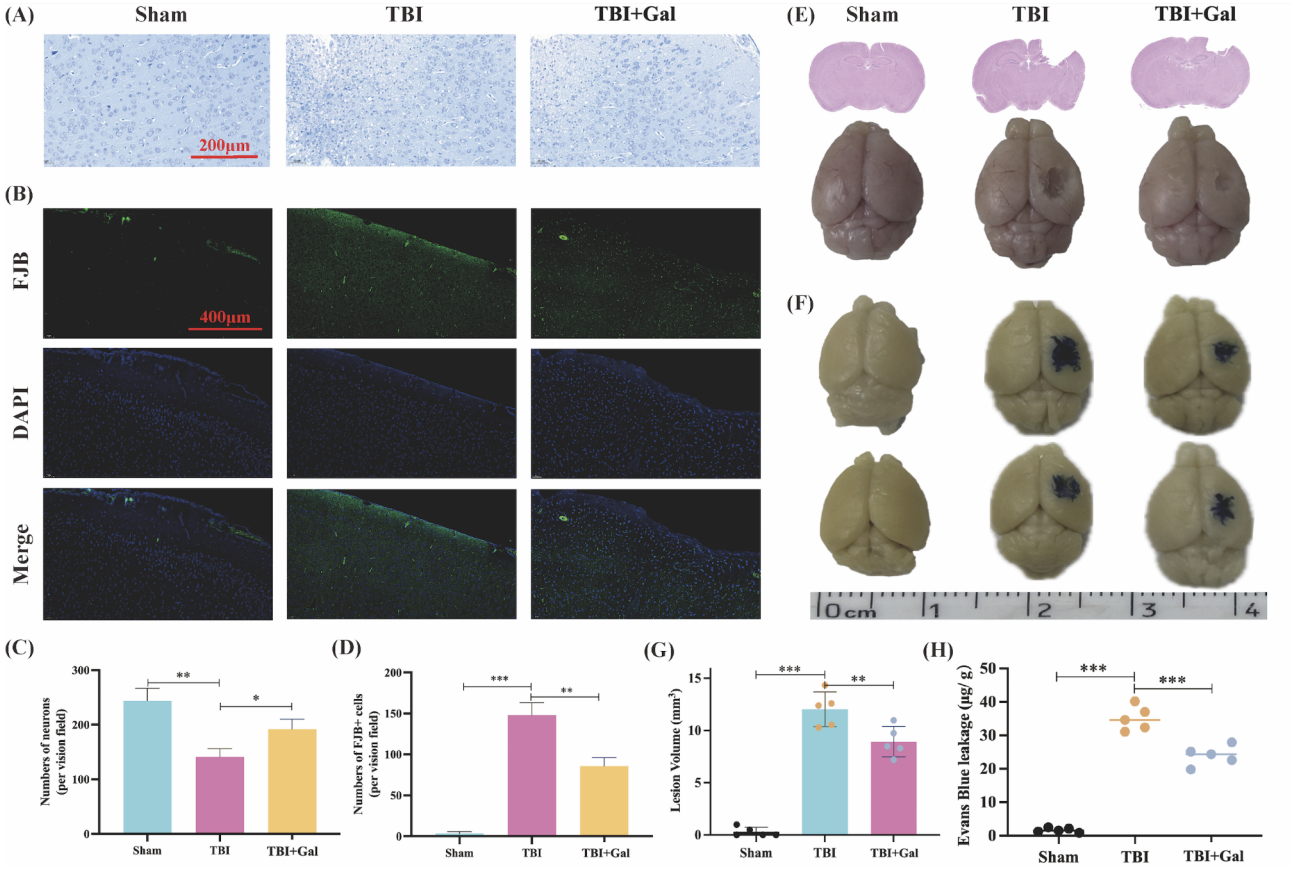

Fig. 4. Gallic acid protects neurons and brain tissue after TBI. (**A**, **C**) Representative images of each group with Nissl staining and their quantitative analysis. (**B**, **D**) The representative images of FJB staining in each group and their quantitative analysis. (**E**, **G**) HE staining and quantitative analysis of tissue defect degree ($n = 5$). (**F**, **H**) Representative pictures of EB extravasation and quantitative analysis of EB leakage ($n = 5$). (*$P < 0.05$, **$P < 0.01$, and ***$P < 0.001$).

score of the Gallic acid treatment group was lower than that of the TBI group, suggesting that Gallic acid treatment can reduce the degree of brain inFig. (Fig. 5B). NORI in mice after TBI was significantly lower than that in normal mice. However, NORI in the Gallic acid treatment group was significantly higher than that in the TBI group, suggesting that Gallic acid can significantly improve the memory and learning ability of mice afterFig. (Fig. 5C). In the Morris water maze experiment, the number of times that mice passed through the hidden platform area in water and the proportion of time spent in the quadrant where the platform was located after TBI were significantly lower than that of normal mice, indicating that the learning ability and memory of mice after TBI were significantly decreased. After Gallic acid treatment, the number of mice crossing the hidden platform region was increased compared with the TBI group, and the proportion of time spent in the quadrant where the platform was located was significantly increased compared with the TBI gFig. (Fig. 5D-F).

Discussion

With the rapid development of social economy, the number of motor vehicles has soared, infrastructure has blossomed everywhere, and brain injuries caused by traffic accidents and falling injuries from high places have also followed[32]. TBI is a disabling injury with a high fatality rate, and most of the patients need surgical treatment for primary brain injury[33,34]. However, in addition to the primary brain injury, the subsequent secondary brain injury, such as inflammation, edema, BBB destruction, and ROS production will continue to cause damage to nerve cells[35–37]. If the secondary injury is not controlled in time, the patient's prognosis will also be worse[38]. Ferroptosis is a newly defined form of cell death in recent years, which plays an important role in the occurrence and development of many diseases, including TBI[39]. Our results on the changes of GPX4, NOX2 and TfR1 expression levels, characteristic changes of mitochondria under electron microscopy and iron deposition levels in brain tissue further prove that ferroptosis is involved in the secondary pathophysiological changes of traumatic brain injury.

Ferroptosis is a new type of iron-dependent programmed cell death, which is different from apoptosis, cell necrosis and autophagy[40]. The main mechanism of ferroptosis is that under the action of ferrobivalent or ester oxygenase, the highly expressed unsaturated fatty acids on the cell membrane are catalyzed to undergo lipid peroxidation, thus inducing cell death[41]. In addition, it also showed a decrease in GPX4, the regulatory core

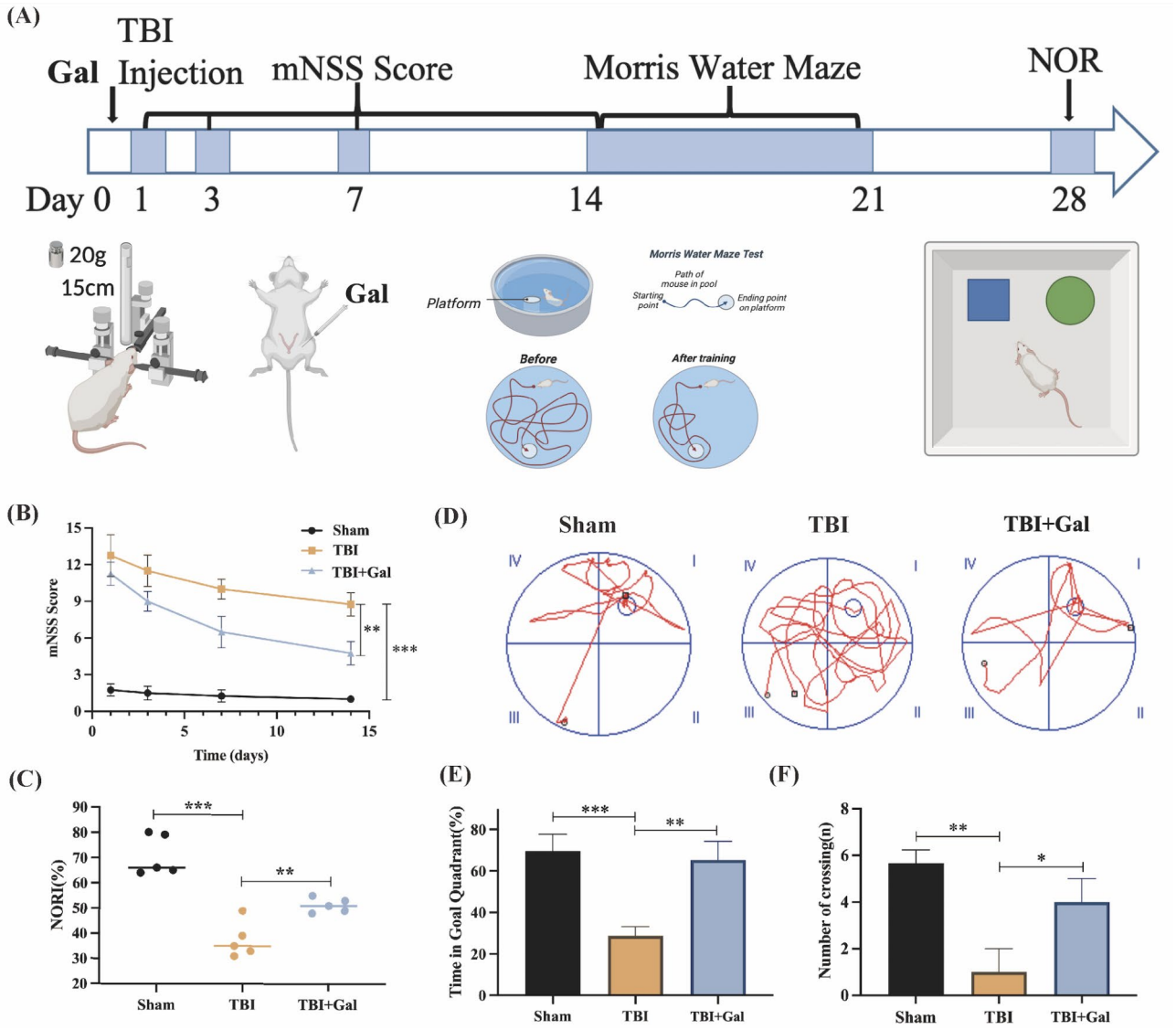

Fig. 5. Gallic acid alleviates behavioral cognitive impairment caused by TBI. (**A**) Behavioral experiment timeline and schematic diagrams. (**B**) mNSS score of each group ($n=5$). (**C**) NORI of each group ($n=5$). (**D**) Representative swimming tracks of mice in each group ($n=5$). (**E**) Quantitative analysis of time proportion in target quadrant ($n=5$). (**F**) Quantitative analysis of the number of crossing platform area ($n=5$). ($^{*}P<0.05$, $^{**}P<0.01$, and $^{***}P<0.001$).

enzyme of the antioxidant system (glutathione system)[42]. There are also characteristic changes in morphology, which are mainly manifested as the shrinkage of the mitochondrial double membrane structure and the disappearance of mitochondrial ridge[43]. Our experimental results also confirm this point.

Both WGCNA and machine-learning algorithms are advanced algorithms for finding key genes in genomics that can quickly help us find core genes in diseases through computers[44]. In this study, we used WGCNA and three machine-learning methods (LASSO, SVM-RFE, RF) to identify the core genes after TBI. We focused on exploring the genes that express proteins and verified them by q-PCR. The bioinformatics analysis was consistent with the experimental results of two genes: APOC3 and KCND3. Then, through functional enrichment of genes and pharmacological prediction through online networks, we found that Gallic acid can act on APOC3, and APOC3 is closely related to ROS, inflammation, lipid metabolism and other physiological and pathological processes. Further experiments are conducted to study the effect of Gallic acid on TBI, mainly to determine whether it can reduce nerve function deficits caused by TBI by inhibiting ferroptosis.

The results showed that Gallic acid inhibited the expression of APOC3 after TBI. PPI analysis showed that APOC3 was closely related to ferroptosis key proteins. In addition, the characteristic ferroptosis manifestations of mitochondria in the brain tissues of mice treated with Gallic acid were reduced under electron microscopy, and the changes in the expression levels of ferroptosis key proteins were also correspondingly reduced, which was also confirmed by immunohistochemistry. Of course, the iron content in the tissues of mice in the Gallic acid group also decreased correspondingly, which jointly confirmed that Gallic acid could reduce the ferroptosis

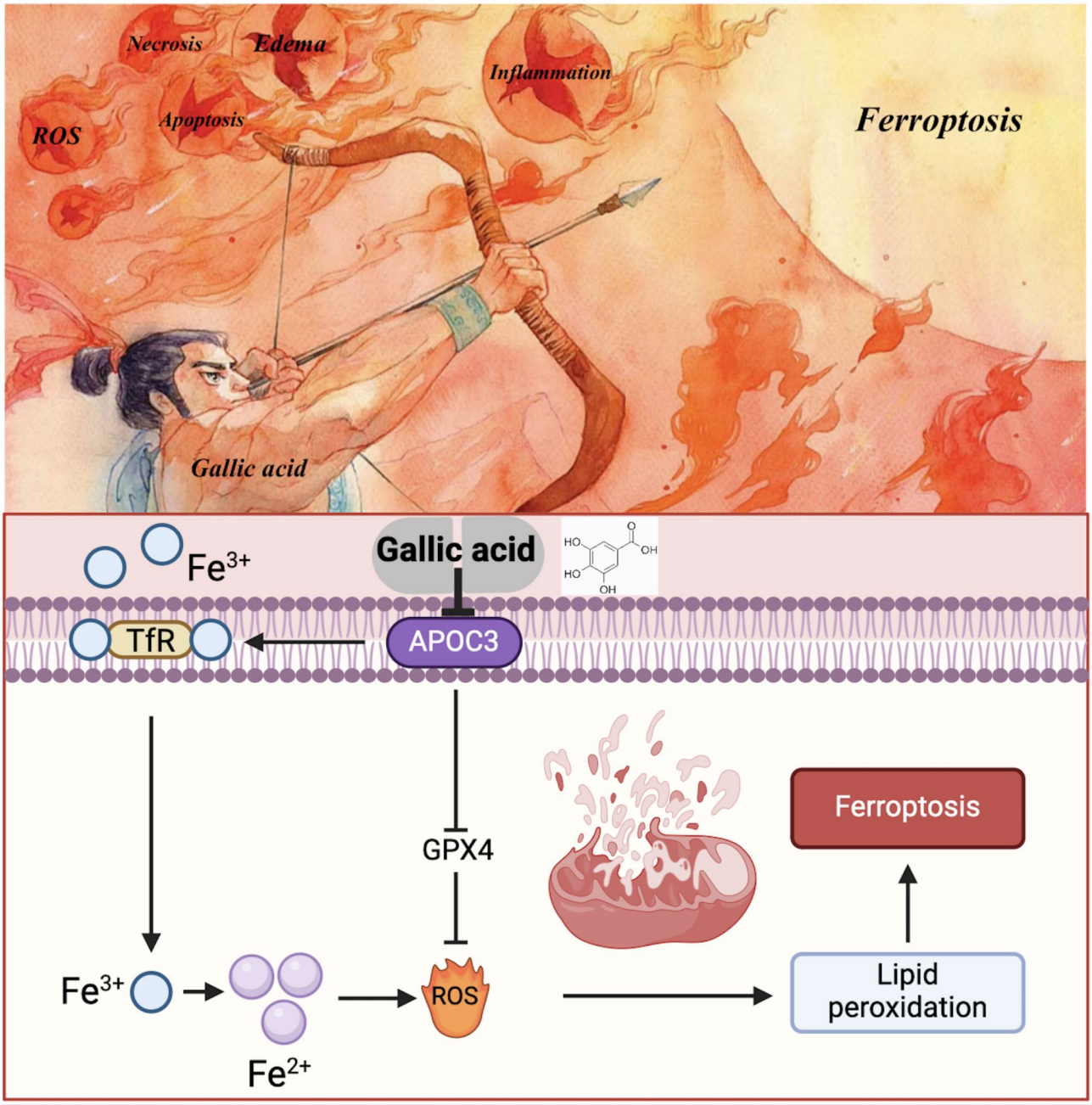

Fig. 6. Schematic diagram of Gallic acid treatment inhibiting TBI-induced ferroptosis.

level. We also found that Gallic acid can reduce brain tissue defects and protect BBB. The results of the behavioral experiments show that Gallic acid can alleviate the neurological impairment caused by TBI. By analyzing the chemical structure formula of Gallic acid, we also found that Gallic acid and curcumin have the same chemical group: Phenol. Phenol can be used in pharmaceutical industry as raw material and additive in pharmaceutical synthesis[45]. For example, parabens have analgesic, anti-inflammatory, antibacterial and other biological activities, and are often used in the preparation of painkillers, anti-inflammatory drugs, anti-inflammatory drugs, etc[46]. It is likely that this is the main group in which Gallic acid exerts its therapeutic effects. We will analyze drugs with similar structures in subsequent studies, focusing on the structures that play the main pharmacological role.

As shoFig. Fig. 6, Gallic acid reduces the accumulation of free iron caused by TBI and the excessive consumption of GPX4 by inhibiting the expression level of APOC3, thus reducing ferroptosis caused by lipid peroxidation. To sum up, Gallic acid can inhibit ferroptosis caused by TBI. Secondly, after Gallic acid treatment, brain tissue defects and BBB damage degree were reduced. Gallic acid treatment reduced nerve necrosis and degenerative changes in mice.

However, it is important to acknowledge that the exact molecular mechanisms linking APOC3 inhibition by Gallic acid to the modulation of GPX4, NOX2, and TfR1 remain incompletely resolved. While our findings

demonstrate correlative associations, causality between APOC3 suppression and downstream ferroptosis-related pathways requires further validation. Future studies utilizing APOC3-specific genetic models or in vitro mechanistic assays are necessary to delineate the precise regulatory interactions and confirm Gallic acid's direct role in this network.

Data availability

The raw data supporting the conclusions of this article will be made available by the corresponding author on request.

Received: 10 July 2024; Accepted: 27 February 2025
Published online: 06 March 2025

References

1. Wilson, J. E. et al. Worse than death: survey of public perceptions of disability outcomes after hypothetical traumatic brain injury. *Ann. Surg.* **273** (3), 500–506. https://doi.org/10.1097/SLA.0000000000003389 (2021).
2. Kundu, S. & Singh, S. What happens in TBI? A wide talk on animal models and future perspective [published online ahead of print, 2022 Jul 6]. *Curr. Neuropharmacol.* https://doi.org/10.2174/1570159X20666220706094248 (2022).
3. Yang, Q. et al. Will sirtuins be promising therapeutic targets for TBI and associated neurodegenerative diseases?? *Front. Neurosci.* **14**, 791. https://doi.org/10.3389/fnins.2020.00791 (2020).
4. Basso, M. & Milelli, A. Transglutaminases, neuronal cell death and neural repair: implications for traumatic brain injury and therapeutics. *Curr. Opin. Neurol.* **32** (6), 796–801. https://doi.org/10.1097/WCO.0000000000000753 (2019).
5. Badhiwala, J. H., Wilson, J. R. & Fehlings, M. G. Global burden of traumatic brain and spinal cord injury. *Lancet Neurol.* **18** (1), 24–25. https://doi.org/10.1016/S1474-4422(18)30444-7 (2019).
6. Davis, C. K. & Vemuganti, R. Antioxidant therapies in traumatic brain injury. *Neurochem Int.* **152**, 105255. https://doi.org/10.1016/j.neuint.2021.105255 (2022).
7. Wei, P. et al. Cordycepin confers long-term neuroprotection via inhibiting neutrophil infiltration and neuroinflammation after traumatic brain injury. J Neuroinflammation. ;18(1):137. Published 2021 Jun 15. (2021). https://doi.org/10.1186/s12974-021-02188-x
8. Wang, Z. et al. Melatonin alleviates intracerebral Hemorrhage-Induced secondary brain injury in rats via suppressing apoptosis, inflammation, oxidative stress, DNA damage, and mitochondria injury. *Transl Stroke Res.* **9** (1), 74–91. https://doi.org/10.1007/s12975-017-0559-x (2018).
9. Zille, M. et al. Neuronal death after hemorrhagic stroke in vitro and in vivo shares features of ferroptosis and necroptosis. *Stroke* **48** (4), 1033–1043. https://doi.org/10.1161/STROKEAHA.116.015609 (2017).
10. Chen, J. et al. Molecular mechanisms of neuronal death in brain injury after subarachnoid hemorrhage. *Front. Cell. Neurosci.* **16**, 1025708. https://doi.org/10.3389/fncel.2022.1025708 (2022).
11. Zhu, X. et al. Nicotinamide mononucleotides alleviated neurological impairment via anti-neuroinflammation in traumatic brain injury. *Int. J. Med. Sci.* **20** (3), 307–317. https://doi.org/10.7150/ijms.80942 (2023).
12. Li, J. et al. Ferroptosis: past, present and future. *Cell. Death Dis.* **11** (2), 88. https://doi.org/10.1038/s41419-020-2298-2 (2020).
13. Ma, T. L. et al. Focus on ferroptosis regulation: exploring novel mechanisms and applications of ferroptosis regulator. *Life Sci.* **307**, 120868. https://doi.org/10.1016/j.lfs.2022.120868 (2022).
14. Gan, B. Mitochondrial regulation of ferroptosis. *J. Cell. Biol.* **220** (9), e202105043. https://doi.org/10.1083/jcb.202105043 (2021).
15. Zhang, Y. et al. Prospects for the role of ferroptosis in fluorosis. *Front. Physiol.* **12**, 773055. https://doi.org/10.3389/fphys.2021.773055 (2021).
16. Gao, Z. et al. Hemin mitigates contrast-induced nephropathy by inhibiting ferroptosis via HO-1/Nrf2/GPX4 pathway. *Clin. Exp. Pharmacol. Physiol.* **49** (8), 858–870. https://doi.org/10.1111/1440-1681.13673 (2022).
17. Lin, W. et al. Ferroptosis is involved in Hypoxic-ischemic brain damage in neonatal rats. *Neuroscience* **487**, 131–142. https://doi.org/10.1016/j.neuroscience.2022.02.013 (2022).
18. Rui, T. et al. Deletion of ferritin H in neurons counteracts the protective effect of melatonin against traumatic brain injury-induced ferroptosis. *J. Pineal Res.* **70** (2), e12704. https://doi.org/10.1111/jpi.12704 (2021).
19. Gao, Y. et al. Melatonin ameliorates neurological deficits through MT2/IL-33/ferritin H signaling-mediated Inhibition of neuroinflammation and ferroptosis after traumatic brain injury. *Free Radic Biol. Med.* **199**, 97–112. https://doi.org/10.1016/j.freeradbiomed.2023.02.014 (2023).
20. Huang, L. et al. Polydatin alleviates traumatic brain injury: role of inhibiting ferroptosis. *Biochem. Biophys. Res. Commun.* **556**, 149–155. https://doi.org/10.1016/j.bbrc.2021.03.108 (2021).
21. Jiang, F., Zhou, H. & Shen, H. Identification of critical biomarkers and immune infiltration in rheumatoid arthritis based on WGCNA and LASSO algorithm. *Front. Immunol.* **13**, 925695. https://doi.org/10.3389/fimmu.2022.925695 (2022).
22. You, J. A. et al. WGCNA, LASSO and SVM algorithm revealed RAC1 correlated M0 macrophage and the risk score to predict the survival of hepatocellular carcinoma patients. *Front. Genet.* **12**, 730920. https://doi.org/10.3389/fgene.2021.730920 (2022).
23. Jiang, Y. et al. Identification of a six-gene prognostic signature for bladder cancer associated macrophage. *Front. Immunol.* **13**, 930352. https://doi.org/10.3389/fimmu.2022.930352 (2022).
24. Fang, S. et al. HERB: a high-throughput experiment- and reference-guided database of traditional Chinese medicine. *Nucleic Acids Res.* **49** (D1), D1197–D1206. https://doi.org/10.1093/nar/gkaa1063 (2021).
25. Mann, S. et al. Evaluation of Anti-inflammatory effects of Choerospondias axillaris fruit's methanolic extract in synoviocytes and CIA rat model. *Curr. Pharm. Biotechnol.* **21** (7), 596–604. https://doi.org/10.2174/1389201021666191210114127 (2020).
26. Das, P. et al. Effect of thermosonication on the nutritional quality of lapsi (Choerospondias axillaris) fruit juice: application of advanced artificial neural networks. *Foods* **12** (20), 3723. https://doi.org/10.3390/foods12203723 (2023).
27. Baraskar, K. et al. Therapeutic role of phytophenol Gallic acid for the cure of COVID-19 pathogenesis. *Endocr. Metab. Immune Disord Drug Targets*. **23** (4), 464–469. https://doi.org/10.2174/1871530322666220829141401 (2023).
28. Sarkaki, A. et al. Gallic acid improved behavior, brain electrophysiology, and inflammation in a rat model of traumatic brain injury. *Can. J. Physiol. Pharmacol.* **93** (8), 687–694. https://doi.org/10.1139/cjpp-2014-0546 (2015).
29. Sun, G. W. et al. Honokiol reduces mitochondrial dysfunction and inhibits apoptosis of nerve cells in rats with traumatic brain injury by activating the mitochondrial unfolded protein response. *J. Mol. Neurosci.* **72** (12), 2464–2472. https://doi.org/10.1007/s12031-022-02089-5 (2022).
30. Liu, Y. et al. Anacardic acid improves neurological deficits in traumatic brain injury by anti-ferroptosis and anti-inflammation. *Exp. Neurol.* **370**, 114568. https://doi.org/10.1016/j.expneurol.2023.114568 (2023).
31. Henry, R. J. et al. Interaction of high-fat diet and brain trauma alters adipose tissue macrophages and brain microglia associated with exacerbated cognitive dysfunction. *J. Neuroinflammation*. **21** (1), 113. https://doi.org/10.1186/s12974-024-03107-6 (2024).
32. Cociu, S. et al. A profile of traumatic brain injury within hospital emergency departments - a retrospective study in the Republic of Moldova. *Open. J. Prev. Med.* **12** (9), 175–189. https://doi.org/10.4236/ojpm.2022.129013 (2022).

33. Zhao, J. et al. Mitochondria transplantation protects traumatic brain injury via promoting neuronal survival and astrocytic BDNF. *Transl Res.* **235**, 102–114. https://doi.org/10.1016/j.trsl.2021.03.017 (2021).
34. Chen, L. et al. The role of coagulopathy and subdural hematoma thickness at admission in predicting the prognoses of patients with severe traumatic brain injury: a multicenter retrospective cohort study from China. *Int. J. Surg.* **110** (9), 5545–5562. https://doi.org/10.1097/JS9.0000000000001650 (2024).
35. Abbasloo, E. et al. Carvacrol decreases blood-brain barrier permeability post-diffuse traumatic brain injury in rats. *Sci. Rep.* **13** (1), 14546. https://doi.org/10.1038/s41598-023-40915-x (2023).
36. Jha, R. M. & Kochanek, P. M. A precision medicine approach to cerebral edema and intracranial hypertension after severe traumatic brain injury: quo vadis?? *Curr. Neurol. Neurosci. Rep.* **18** (12), 105. https://doi.org/10.1007/s11910-018-0912-9 (2018).
37. Chen, Y. et al. WTAP participates in neuronal damage by protein translation of NLRP3 in an m6A-YTHDF1-dependent manner after traumatic brain injury. *Int. J. Surg.* **110** (9), 5396–5408. https://doi.org/10.1097/JS9.0000000000001794 (2024).
38. Roberson, S. W. et al. Challenges of delirium management in patients with traumatic brain injury: from pathophysiology to clinical practice. *Curr. Neuropharmacol.* **19** (9), 1519–1544. https://doi.org/10.2174/1570159X19666210119153839 (2021).
39. Rui, T. et al. Ferroptosis-relevant mechanisms and biomarkers for therapeutic interventions in traumatic brain injury. *Histol. Histopathol.* **35** (10), 1105–1113. https://doi.org/10.14670/HH-18-229 (2020).
40. Dixon, S. J. et al. Ferroptosis: an iron-dependent form of nonapoptotic cell death. *Cell* **149** (5), 1060–1072. https://doi.org/10.1016/j.cell.2012.03.042 (2012).
41. Dierge, E. et al. Peroxidation of n-3 and n-6 polyunsaturated fatty acids in the acidic tumor environment leads to ferroptosis-mediated anticancer effects. *Cell. Metab.* **33** (8), 1701–1715e5. https://doi.org/10.1016/j.cmet.2021.05.016 (2021).
42. Ursini, F. & Maiorino, M. Lipid peroxidation and ferroptosis: the role of GSH and GPx4. *Free Radic Biol. Med.* **152**, 175–185. https://doi.org/10.1016/j.freeradbiomed.2020.02.027 (2020).
43. Liu, Y. et al. The diversified role of mitochondria in ferroptosis in cancer. *Cell. Death Dis.* **14** (8), 519. https://doi.org/10.1038/s41419-023-06045-y (2023).
44. Xu, M. et al. Identification and validation of immune and oxidative stress-related diagnostic markers for diabetic nephropathy by WGCNA and machine learning. *Front. Immunol.* **14**, 1084531. https://doi.org/10.3389/fimmu.2023.1084531 (2023).
45. Podili, R. et al. Design, synthesis, and histone deacetylase Inhibition study of novel 4-(2-aminoethyl) phenol derivatives. *J. Biochem. Mol. Toxicol.* **38** (1), e23591. https://doi.org/10.1002/jbt.23591 (2024).
46. Gopal, C. M. et al. Evaluation of selected pharmaceuticals and personal care products in water matrix using ion trap mass spectrometry: A simple weighted calibration curve approach. *J. Pharm. Biomed. Anal.* **185**, 113214. https://doi.org/10.1016/j.jpba.2020.113214 (2020).

Acknowledgements

This work was financially supported by Postgraduate Research&Practice Innovation Program of Jiangsu Province (SJCX23-1413). This work was supported by the Huai'an Science and Technology Plan Project (No. HAB202321).

Author contributions

Yu Liu and Xiaojia Fu wrote the main manuscript text. Jing Li and Jianqiang Guo visualized the figures. Zongren Zhao and Jinyu Zheng reviewed and edited the final manuscript. All authors reviewed the manuscript.

Declarations

Competing interests

The authors declare no competing interests.

Additional information

Supplementary Information The online version contains supplementary material available at https://doi.org/10.1038/s41598-025-92383-0.

Correspondence and requests for materials should be addressed to Z.Z. or J.Z.